Journal of Biomedical Optics

SPIEDigitalLibrary.org/jbo

Photoacoustic needle: minimally invasive guidance to biopsy

Daniele Piras
Chiel Grijsen
Peter Schütte
Wiendelt Steenbergen
Srirang Manohar

SPIE

Photoacoustic needle: minimally invasive guidance to biopsy

Daniele Piras, Chiel Grijsen, Peter Schütte, Wiendelt Steenbergen, and Srirang Manohar
University of Twente, Biomedical Photonic Imaging Group, MIRA Institute, P.O. Box 217, 7500AE Enschede, The Netherlands

Abstract. We introduce a needle probe based on photoacoustics (PA) to extend the scope of optical needle methods in guiding biopsies. Pulsed light is coupled to an optical fiber in a needle to be inserted in tissue, and PA signals are detected using an ultrasound imager used for needle guidance. This PA needle samples large volumes and possesses an imaging component so that sites forward and off-axis of the fiber are surveyed. This allows navigation of those regions for optical characterization and direct biopsy in a subsequent step. The concept is explored on simple phantoms and biological specimens. [DOI: 10.1117/1.JBO.18.7.070502]

Keywords: photoacoustic; ultrasound; biopsy.

Paper 130250LR received Apr. 17, 2013; revised manuscript received May 27, 2013; accepted for publication May 30, 2013; published online Jul. 1, 2013.

Biopsy is the gold standard for diagnosis of cancer in organs like the breast.[1] Samples are extracted through a needle under ultrasound (US) or stereotactic x-ray imaging. The size of samples is a few cubic millimeters in core needle biopsy (CNB). Samples are histologically examined for the presence of cancer cells and, if positive, tumor type and grade are ascertained. Further, vascular channel invasion and molecular markers are ascertained.[2] However, imaging methods have drawbacks: US and x-ray imaging suffer from limited sensitivity and specificity, and needle visualization is poor in US.[3] Coupled with the spatial heterogeneity of cancers, the sampled tissue may not be representative of the pathology: cancers are missed in 4.3% to 17.9%, and repeat biopsies are needed in 4% to 32% of cases.[4] Optical fiber-based probes that insert into biopsy needles have been developed[5] and can provide spectroscopic assessment of tissue to guide the biopsy in a further step. These techniques rely on wavelength-dependent differences in optical properties between cancerous and normal tissues.[5] Optical properties are estimated by fitting models of photon propagation in tissue using *a priori* knowledge of the spectral behavior of expected chromophores. The estimated absorption and reduced scattering coefficients are indicative of physiological and structural properties averaged over volumes not exceeding 5 to 10 mm^3.

Address all correspondence to: Daniele Piras, University of Twente, Biomedical Photonic Imaging Group, MIRA Institute, P.O. Box 217, 7500AE Enschede, The Netherlands. Tel: +31-53-489 3877; Fax: +31-53-489 1105; E-mail: d.piras@utwente.nl

We aim to extend the scope of the optical method by sampling larger volumes of tissue for optical properties, while attaching spatial information to this contrast. We add an imaging component to the method so that the sites forward and off-axis of the fiber tip are surveyed by using photoacoustics (PA). The method has the advantage of high optical absorption contrast possible in optical imaging, and high spatial resolution associated with US. Light absorption, followed by fast nonradiative de-excitation and temperature rise, leads to localized thermoelastic expansion. The resulting pressure waves propagate to the tissue surface and are registered using US transducers.[6,7] In our concept, the PA needle, we use pulsed light in a fiber-based needle probe to excite PA waves in the vicinity of a lesion. Light is delivered inside the tissue in contrast with noninvasive PA imaging for biopsy guidance.[3] The excitation is close to the region of interest, reducing light losses, while adapting to the setting of biopsy. The US imager used for needle guidance performs PA detection. To demonstrate feasibility, we present first results in phantoms and biological specimens. A first estimation of optical properties is performed, while demonstrating the imaging capabilities.

The system (Fig. 1) consists of a US imager (Picus, Esaote Europe BV, Maastricht) with a linear array transducer L10-5 (128 elements, 7.5 MHz, 75% bandwidth).[7] A multimode optical fiber (NA 0.22, diameter 600 μm) delivers 10 ns laser light at 1064 nm (Diny pQ, IB laser, Berlin) with 1.4 mJ/pulse at 250 Hz. The PA frame rate is 2 Hz and images are reconstructed online with a phased-array algorithm. The fiber is held in a metal housing (biopsy needle 14 G × 13 cm, Bard Ltd, UK) and fixed with Stycast discs (Fig. 1). Finally it slide-fits into a 14 G cutting cannula. A 2-mm cube of poly(vinyl alcohol) (PVA) (Table 1) is used as insert, held on a nylon thread and submerged in a liquid bath at 5 cm from the transducer. The bath contains solutions of Intralipid 20% (Fresenius Kabi, Germany) and Intralipid/Ecoline Black (nr. 700, Royal Talens, The Netherlands), with optical properties shown in Table 1. The PA needle is moved at a 45-deg orientation towards the insert. PA frames are acquired at several distances (18 averages, 10 to 20 frames, 0.5 mm step) between the fiber tip and insert.

In Fig. 2, results for experiment A are shown. In each frame [Fig. 2(a)] we see high intensity from the fiber tip (PA_{fib}) and from the insert (PA_{ins}). In Fig. 2(b), all frames are summed up: we observe the trace of PA_{fib} along the 45-deg path. The insert is visualized, though the front face dominates due to the higher fluence at that point and to the limited bandwidth of the transducer (Fig. 2, insets). In Fig. 2(b) (inset) front and back surfaces of the insert are seen 2 mm apart. For each frame rectangular ROIs including insert and fiber signals are selected. The fiber to insert distance (r) is defined as the distance between the coordinates of maximum signal (PA_{max}) in the two ROIs. Average values of PA_{ins} and PA_{fib} are calculated in a −6 dB threshold with respect to PA_{max}, and plotted against r. In Fig. 2(c), curves for experiment A are reported. With decreasing r, PA_{ins} increases, while PA_{fib} is constant, except for a steep increase close to the insert.

Under diffusion approximation, with $\mu_{a,m}$ and $\mu'_{s,m}$ medium optical properties, and $\mu_{a,ins}$ insert absorption coefficient, for every r_i along the needle axis, the insert absorbed energy density $E_{a,ins}$ can be written as

$$E_{a,\mathrm{ins}}(r_i) = \Phi_0 \left[\frac{\exp(-\mu_{\mathrm{eff},m} r_i)}{r_i}\right] \mu_{a,\mathrm{ins}}, \qquad (1)$$

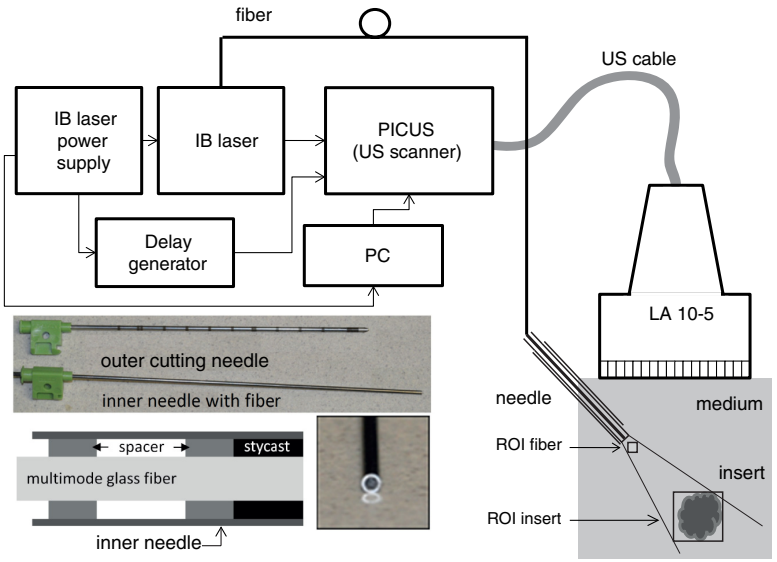

Fig. 1 Schematic of the PA imaging experimental setup with the selection of the region of interest (ROI) for fiber tip and insert. The outer and inner needles are shown in the insets.

where Φ_0 is the fluence at the fiber interface and $\mu_{\mathrm{eff},m} = \sqrt{3\mu_{a,m}(\mu_{a,m} + \mu'_{s,m})}$ is the medium effective attenuation coefficient. We assume that $\mathrm{PA}_{\mathrm{fib}}$ is constant for every position of the needle along its trajectory. This first approximation for the simple phantoms used will lose validity in the case of optical heterogeneity. In future work, a model-based approach can avoid this assumption. By fitting Eq. (1) to the experimental data, we obtain $\mu_{\mathrm{eff},m}$.[8] For experiments A (nine measurements) we report mean and standard deviation of estimated $\mu_{\mathrm{eff},m}$, for experiments B and C (one measurement each) we report the estimated $\mu_{\mathrm{eff},m}$ with 95% confidence bounds (Table 1). Good agreement between actual and estimated $\mu_{\mathrm{eff},m}$ is found (Table 1), with error less than 20%. It is possible to quantify $\mu_{\mathrm{eff},m}$ of a homogeneous medium in a large probing volume

Table 1 Optical properties (absorption coefficient μ_a, reduced scattering coefficient μ'_s, and effective attenuation coefficient μ_{eff}) of the poly(vinyl alcohol) insert (subscript ins) and of the embedding medium (subscript m), and estimated values for μ_{eff} (all values in mm^{-1}). *95% confidence level bounds. IL, IntraLipid; EB, Ecoline Black.

		Insert	Medium (actual)			Medium (estimated)
Medium composition		$\mu_{a,\mathrm{ins}}$	$\mu_{a,m}$	$\mu'_{s,m}$	$\mu_{\mathrm{eff},m}$	$\mu_{\mathrm{eff},m}$
(A)	3.5%IL20%	0.250	0.0122	0.5	0.137	0.139 ± 0.018
(B)	3.5%IL20% + 0.1%EB	0.250	0.03	0.5	0.218	0.261 ± 0.087*
(C)	3.5%IL20% + 0.2%EB	0.250	0.06	0.5	0.317	0.335 ± 0.354*

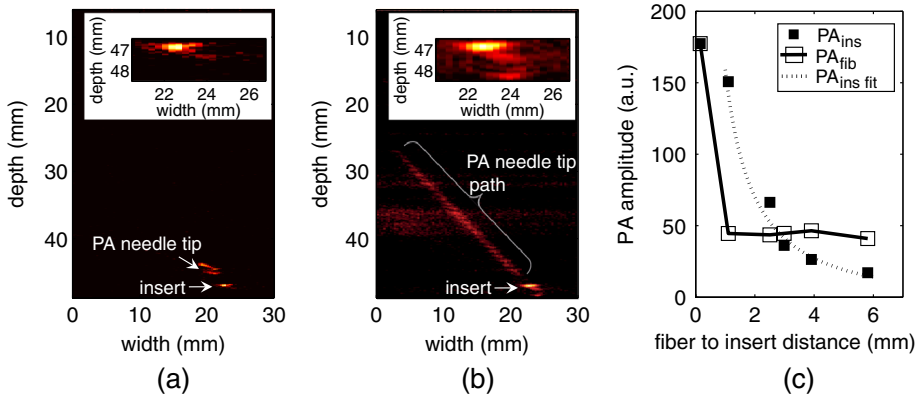

Fig. 2 PA measurement of poly(vinyl alcohol) insert in scattering liquid medium (experiment A in Table 1): (a) single frame, (b) sum of all frames. The insert is enlarged in the insets in (a) and (b). (c) $\mathrm{PA}_{\mathrm{ins}}$ (measurements and fit) and $\mathrm{PA}_{\mathrm{fib}}$ (measurements) against fiber tip to insert distance.

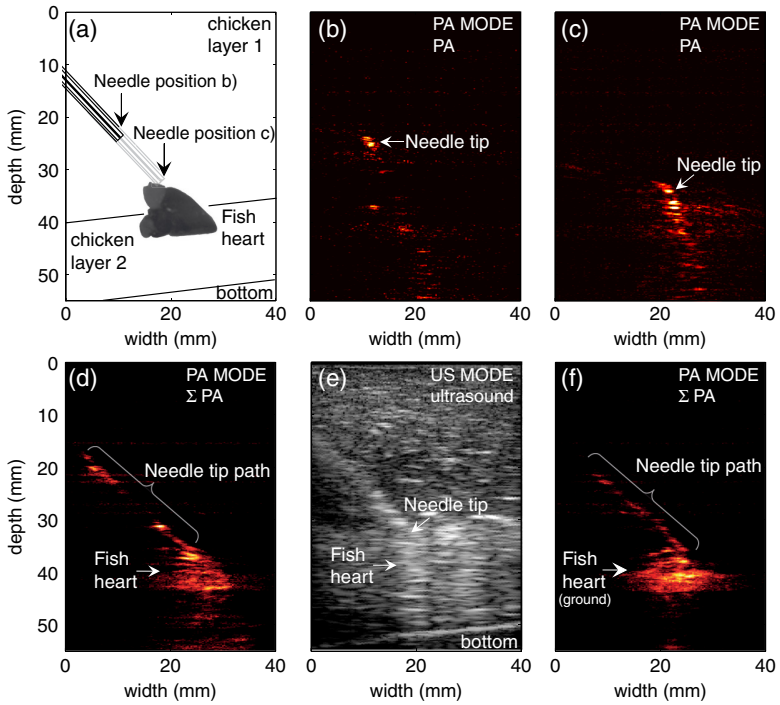

Fig. 3 PA measurement of a fish heart in chicken breast medium: (a) schematic of the measurements with a picture of the fish heart, (b) and (c) single frames at two different fiber depths, (d) sum of all individual frames, (e) ultrasound image, (f) sum of all individual frames after grinding the fish heart.

(at least 5 mm on axis) and obtain location and size of the insert.

To further demonstrate the imaging capability we used chicken breast as a background material, and a $1.5 \times 1.5 \times 0.5$ cm^3 blood rich heart of a fish (*Sparus aurata*) as insert [Fig. 3(a)]. Figure 3(a) shows the schematic of the experiment. Figure 3(b) and 3(c) shows two frames for two positions of the PA needle. Apart from the bright PA_{fib}, PA intensities from the chicken breast are visible in Fig. 3(b). In Fig. 3(c), we see a heterogeneous distribution of high intensity spots where the heart is located. No remarkable US reflections can be recognized. Summing up all PA frames [Fig. 3(d)] we see the path of the needle, and an extended high intensity PA region at the heart location. US confirms the position of the needle and heart [Fig. 3(e)]: the heart is moderately more echogenic than the chicken breast (1.14 contrast), and the needle is barely visible (1.12 contrast). The heart is then ground into small structures to represent the heterogeneities of a tumor.[9] The PA image is shown in Fig. 3(f). PA contrast is better than US contrast in all cases: 34% higher for intact heart; 48% higher for ground heart (US not shown), and 17% higher for the needle.

In summary, we introduced the PA needle concept and have shown that it can supplement optical property estimation, in a minimally invasive setting, with imaging capabilities. The needle is identified in PA with superior visibility to US imaging. We derived $\mu_{\mathrm{eff},m}$ when forward lying absorbing targets are probed. A ground fish heart representing a heterogeneous cancer is imaged in a challenging biological medium: at this stage, we cannot exclude that US reflections from the tip affect the PA images at the position of the heart. We intend to work on a model-based approach to invert a forward model by iteratively fitting it to the PA measurements. With instrumental improvements[10] and multiple wavelengths[11] it might make possible quantitation of $\mu_{a,\mathrm{ins}}$ and $\mu_{a,m}$, providing powerful discrimination capabilities for guiding biopsy in breast care.

Acknowledgments

This work was supported by the AgentschapNL-IOP (HYMPACT IPD083374) and the High Tech Health Farm (HTHF) of the province of Overijssel. Dr. Peter Brands (Esaote Europe BV) is thanked for discussions and support with the Picus imager.

References

1. American Cancer Society, *Cancer Facts & Figures 2012*, pp. 1–64, American Cancer Society, Atlanta (2012).
2. H. Denley et al., "Preoperative assessment of prognostic factors in breast cancer," *J. Clin. Pathol.* **54**(1), 20–24 (2001).
3. C. Kim et al., "Handheld array-based photoacoustic probe for guiding needle biopsy of sentinel lymph nodes," *J. Biomed. Opt.* **15**(4), 046010 (2010).
4. R. Nachabé et al., "Diagnosis of breast cancer using diffuse optical spectroscopy from 500 to 1600 nm: comparison of classification methods," *J. Biomed. Opt.* **16**(8), 087010 (2011).
5. D. J. Evers et al., "Optical spectroscopy: current advances and future applications in cancer diagnostics and therapy," *Future Oncol.* **8**(3), 307–320 (2012).
6. M. Heijblom et al., "Visualizing breast cancer using the Twente photoacoustic mammoscope: what do we learn from twelve new patient measurements?," *Opt. Express* **20**(11), 11582–11597 (2012).
7. R. G. M. Kolkman et al., "Real-time *in vivo* photoacoustic and ultrasound imaging," *J. Biomed. Opt.* **13**(5), 050510 (2008).
8. S. A. Telenkov and A. Mandelis, "Photothermoacoustic imaging of biological tissues: maximum depth characterization comparison of time and frequency-domain measurements," *J. Biomed. Opt.* **14**(4), 044025 (2009).
9. L. V. Wang and S. Hu, "Photoacoustic tomography: *in vivo* imaging from organelles to organs," *Science* **335**(6075), 1458–1462 (2012).
10. M. Jaeger et al., "Deformation-compensated averaging for clutter reduction in epiphotoacoustic imaging *in vivo*," *J. Biomed. Opt.* **17**(6), 066007 (2012).
11. J. Laufer et al., "Quantitative spatially resolved measurement of tissue chromophore concentrations using photoacoustic spectroscopy: application to the measurement of blood oxygenation and haemoglobin concentration," *Phys. Med. Biol.* **52**(1), 141–168 (2007).